Adaptive boundaryless finite-difference method

Dorilian Lopez-Mago* and Julio C. Gutiérrez-Vega

Photonics and Mathematical Optics Group, Tecnológico de Monterrey, Monterrey 64849, Mexico
**Corresponding author: dorilian@itesm.mx*

Received November 20, 2012; revised January 11, 2013; accepted January 14, 2013;
posted January 14, 2013 (Doc. ID 180119); published January 31, 2013

The boundaryless beam propagation method uses a mapping function to transform the infinite real space into a finite-size computational domain [Opt. Lett. **21**, 4 (1996)]. This leads to a bounded field that avoids the artificial reflections produced by the computational window. However, the method suffers from frequency aliasing problems, limiting the physical region to be sampled. We propose an adaptive boundaryless method that concentrates the higher density of sampling points in the region of interest. The method is implemented in Cartesian and cylindrical coordinate systems. It keeps the same advantages of the original method but increases accuracy and is not affected by frequency aliasing. © 2013 Optical Society of America

OCIS codes: 350.5500, 070.7345, 080.1510, 000.4430.

1. INTRODUCTION

The numerical propagation of wave fields is limited by the boundaries of the computational window, which leads to artificial reflections that interfere with the propagating wave. It is important to use boundary conditions that absorb the outgoing waves. An artificial absorber is usually inserted adjacent to the computational window boundaries [1]. However, it requires a smooth absorption transition in order to reduce spurious reflections. This condition produces large absorbers that increase memory requirement.

Other methods include the transparent boundary condition and the perfectly matched layer [2,3]. The former modifies the parameters of the waves near the boundaries to represent outgoing plane waves at a given angle of incident. The method is highly successful, but fails in cases where the field is highly diverging. In the perfectly matched layer, a specially designed anisotropic medium is put at the edge of the window.

Ladouceur proposed the boundaryless method as an alternative to solve the boundary condition imposed by the computational domain [4]. The method maps the infinite transverse coordinates in the real space into a finite-size computational domain. The modified wave equation can be efficiently solved by finite-difference beam propagation methods (FD-BPMs). This modification avoids the implementation of absorbing boundary conditions and provides a fast and simple algorithm.

The boundaryless method has been applied with the wide-angle FD-BPM using the generalized Douglas scheme [5], in three-dimensional propagation of paraxial optical wave fields [6], in the solution of the propagation modes in optical dielectric waveguides [7], and long-range plasmonic waveguides [8].

Nevertheless, the method suffers from frequency aliasing problems. The mapping function densely discretizes the central region of the physical domain and scarcely discretizes the exterior. Tilted beams moving outward into the scarcely sample region experience frequency aliasing and tend to return to the center.

In order to overcome this problem, we propose an adaptive mapping function. This mapping densely discretizes the region of high-amplitude field at each propagation step. It offers a real boundaryless method, with better accuracy and without reflections from frequency aliasing. We apply this scheme to propagate tilted wave fields in Cartesian coordinates and compare the results with their analytic solutions. We show the advantages of the adaptive method over the standard method. The implementation in cylindrical coordinates is shown in the Appendix.

2. ADAPTIVE BOUNDARYLESS SCHEME

For referring purposes and to establish notation, let us briefly review the original boundaryless method for $(1+1)$D beams (x,z). The method maps the infinite x coordinate into a finite-size domain by the function

$$x = \alpha \tan\theta, \tag{1}$$

where α is a scaling factor that controls the sampling. The variable θ has the range $[-\pi/2, \pi/2]$. Alternative mapping functions could be used, but this mapping leads to a simplified wave equation and has an elegant geometric interpretation. Notice that Eq. (1) can be regarded as a stereographic projection, where the center of the physical domain corresponds to the north pole of the sphere and the infinity corresponds to the south pole, as shown in Fig. 1(b). Propagating fields are bounded in the finite area of this sphere.

As shown in Fig. 1(a), the mapping transforms a nonuniform grid in the physical domain into a uniform grid in the computational domain. This transformation makes the implementation suitable for finite-difference methods. Using the mapping function in Eq. (1), the density of sampling points is a maximum in the north pole of the sphere and tends to zero in the south pole. Therefore, the field located close to $\theta = 0$ is densely discretized but scarcely discretized away from the center. This mapping is particularly useful when the high-field amplitude propagates along the optical axis, e.g., in optical fibers. Nevertheless, in those cases the computational boundary conditions are not a major problem.

The mapping function in Eq. (1) is not suitable to represent tilted wave fields. When they move outward into the physical

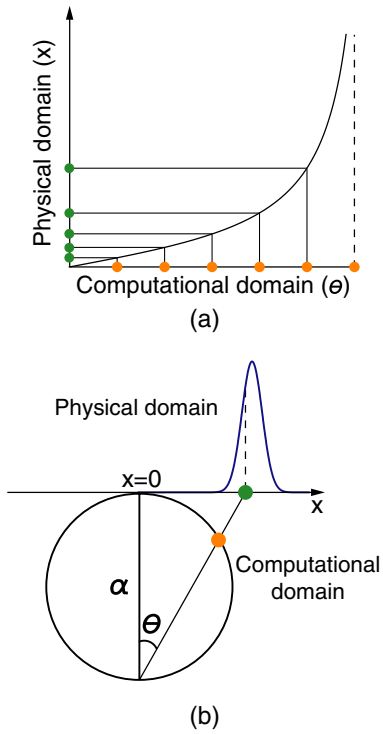

Fig. 1. (Color online) (a) Mapping function $x = \alpha \tan\theta$. This mapping densely discretizes the center of the physical domain but scarcely discretizes the exterior. (b) Geometric interpretation of the mapping function, equivalent to a stereographic projection.

space that is scarcely sampled, they suffer from frequency aliasing, which produces undesired reflections. The maximum sampling separation to avoid frequency aliasing is $\Delta x = \pi/k_t$, where k_t is the transverse wavenumber. Therefore, the available physical space is limited by this condition.

An adaptive sampling would locate the maximum density of points in the region of interest. The density of sampling points is given by $\theta' = d\theta/dx$. The maximum value of θ' is located in the inflection point of the mapping function $x(\theta)$. From Eq. (1), the inflection point is located at $\theta = 0$, which concentrates the sampling points along the propagation axis.

Our adaptive method is implemented by relocating the inflection point of $x(\theta)$ at each propagation step. In order to do that, we generalize Eq. (1) in the following form:

$$x(\theta) = x_0 + \alpha \tan(\theta - \theta_0), \tag{2}$$

where x_0 is the location of interest in the physical domain and the offset $\theta_0 = \tan^{-1}(x_0/\alpha)$ ensures the condition $x(\theta = 0) = 0$. As shown in Fig. 2, the value x_0 could be the position of high-field amplitude or the variance of the energy distribution.

This modification provides an efficient sampling by keeping the simplicity of the method. Furthermore, if the field propagates mostly along the optical axis, the method is essentially equivalent to the original.

3. APPLICATION IN TWO-DIMENSIONAL PARAXIAL OPTICAL BEAMS

We apply the adaptive method to solve the two-dimensional scalar Helmholtz equation in the paraxial approximation

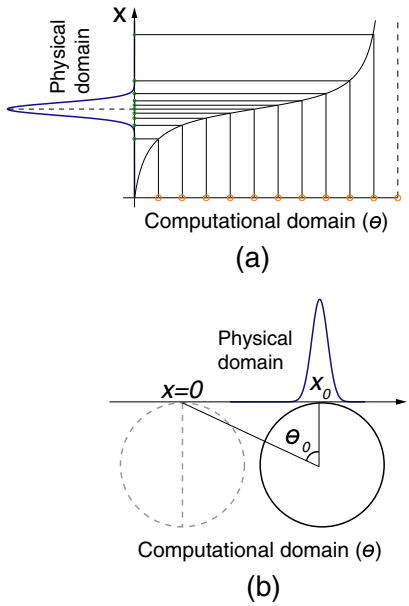

Fig. 2. (Color online) (a) Adaptive function $x(\theta) = x_0 + \alpha \tan(\theta - \theta_0)$, densely discretizes the region in the physical domain where the field is concentrated. (b) Geometric interpretation in terms of a stereographic projection.

$$\frac{\partial^2 U(x,z)}{\partial x^2} + 2ik\frac{\partial U(x,z)}{\partial z} = 0, \tag{3}$$

where $U(x,z)$ is the complex amplitude of the electric field $E(x,z) = U(x,z)\exp(ikz)$. Using the mapping function in Eq. (2) and the field transformation

$$U = \sqrt{\alpha}\sec(|\theta| - \theta_0)\psi(x,z), \tag{4}$$

we get the modified equation

$$\frac{1}{\alpha^2}\cos(|\theta| - \theta_0)^4\frac{\partial^2\psi}{\partial\theta^2} + \frac{1}{\alpha^2}\cos(|\theta| - \theta_0)^4\psi + 2ik\frac{\partial\psi}{\partial z} = 0. \tag{5}$$

Note that Eq. (5) has no terms involving first derivatives of ψ. The field transformation, Eq. (4), is particularly chosen to eliminate the term involving the first derivative of ψ. We take the absolute value of θ to take into account the negative values.

An advantage of the boundaryless method is that in the computational domain, the grid has an uniform sampling. This allows one to solve the modified Eq. (5) using a standard finite-difference scheme. We use the implicit Crank–Nicolson method, which is second-order accurate in both time and space and unconditionally stable [9,10].

We use the following notation

$$\theta_p \equiv p\Delta\theta, \qquad p = 0, 1, \ldots, N-1, \tag{6}$$

$$\psi_p^{(n)} \equiv \psi(\theta_p, n\Delta z), \qquad n = 0, 1, 2, \ldots, \tag{7}$$

where N is the number of sampling points and $\Delta\theta$ and Δz are the sampling interval and propagation step, respectively. After rearranging terms, we arrive to the following tridiagonal system of equations:

$$a_p\psi_{p-1}^{(n+1)} + \left(b_p + i\frac{4k}{\Delta z}\right)\psi_p^{(n+1)} + a_p\psi_{p+1}^{(n+1)} = -a_p\psi_{p-1}^{(n)} - \left(b_p - i\frac{4k}{\Delta z}\right)\psi_p^{(n)} - a_p\psi_{p+1}^{(n)} \tag{8}$$

with

$$a_p = \frac{\cos(|\theta_p| - \theta_0)^4}{\alpha^2\Delta\theta^2}, \tag{9}$$

$$b_p = (\Delta\theta^2 - 2)a_p, \tag{10}$$

which can be solved by matrix inversion and multiplication using

$$\mathbf{\Psi}^{(n+1)} = \mathbf{M}_L^{-1}\mathbf{M}_R\mathbf{\Psi}^{(n)}, \tag{11}$$

$$\mathbf{M}_L = \mathbf{C} + \frac{4ik}{\Delta z}\mathbf{I}_N, \qquad \mathbf{M}_R = -\mathbf{C} + \frac{4ik}{\Delta z}\mathbf{I}_N, \tag{12}$$

where $\mathbf{I}_N$ is a $N \times N$ identity matrix. The tridiagonal matrix $\mathbf{C}$ and the solution vector $\mathbf{\Psi}$ are explicitly

$$\mathbf{C} = \begin{bmatrix} b_0 & a_0 & 0 & \dots & 0 & 0 \\ a_1 & b_1 & a_1 & 0 & \dots & 0 \\ 0 & \ddots & \ddots & \ddots & \ddots & 0 \\ \vdots & \ddots & a_{N-3} & b_{N-3} & a_{N-3} & \vdots \\ 0 & \dots & 0 & a_{N-2} & b_{N-2} & a_{N-2} \\ 0 & 0 & \dots & 0 & a_{N-1} & b_{N-1} \end{bmatrix},$$

$$\mathbf{\Psi}^{(n)} = \begin{bmatrix} \psi_0^{(n)} \\ \psi_1^{(n)} \\ \vdots \\ \psi_{N-3}^{(n)} \\ \psi_{N-2}^{(n)} \\ \psi_{N-1}^{(n)} \end{bmatrix}. \tag{13}$$

We test the algorithm by propagating a cosine-Gauss beam, whose distribution at the initial plane $z = 0$ is given by

$$U(x, 0) = \exp(-x^2/w_0^2)\cos(k_t x), \tag{14}$$

where w_0 is the spot waist and k_t is the transverse wavenumber. The cosine-Gauss beam is a special case of the Helmholtz–Gauss beams and its analytical solution on propagation is well known [11]. The cosine-Gauss propagates pseudo-addiffractionally during a short distance and eventually propagates as two tilted Gaussian beams. This is particularly useful to illustrate the performance of our adaptive method.

For the numerical implementation, we assume $w_0 = 1$ mm, $k_t = 8 \times 10^{-4}k$, and $k = 2\pi/\lambda$ with $\lambda = 632.8$ nm. The θ space is sampled with $N = 500$ and a propagation step of about $\Delta z \approx 5$ mm. Mapping parameter $\alpha = 4w_0$. The finite difference representation of $\psi(x, 0)$ at the plane $z = 0$ is

$$\psi_p^{(0)} = \frac{1}{\sqrt{\alpha}}\exp(-x_p^2/w_0^2)\cos(k_t x_p)\cos(\theta_p), \tag{15}$$

where $x_p \equiv x(\theta_p)$. We compare the results of our adaptive method with the static method ($x_0 = 0$ and $\theta_0 = 0$ at each propagation step). Figure 3 shows the results of both methods after a propagation distance of $z_R = 4.96$ m. Figures 3(a) and 3(b) show the results of $|U|^2$ at the planes $z = 0$ and $z = z_R$, respectively, using the adaptive method. The numerical result shows good agreement with the analytical solution. The performance of the solution could be improved by using, e.g., a Padé scheme for wide-angle propagation [12].

The accuracy is measured by the overlap integral between the numerical result and the analytical solution using [13]

$$\mathrm{ERR} = 1 - \frac{\left|\int U_{\mathrm{exact}}^* U_{\mathrm{computed}}\mathrm{d}x\right|^2}{\int |U_{\mathrm{input}}|^2\mathrm{d}x \int |U_{\mathrm{exact}}|^2\mathrm{d}x}, \tag{16}$$

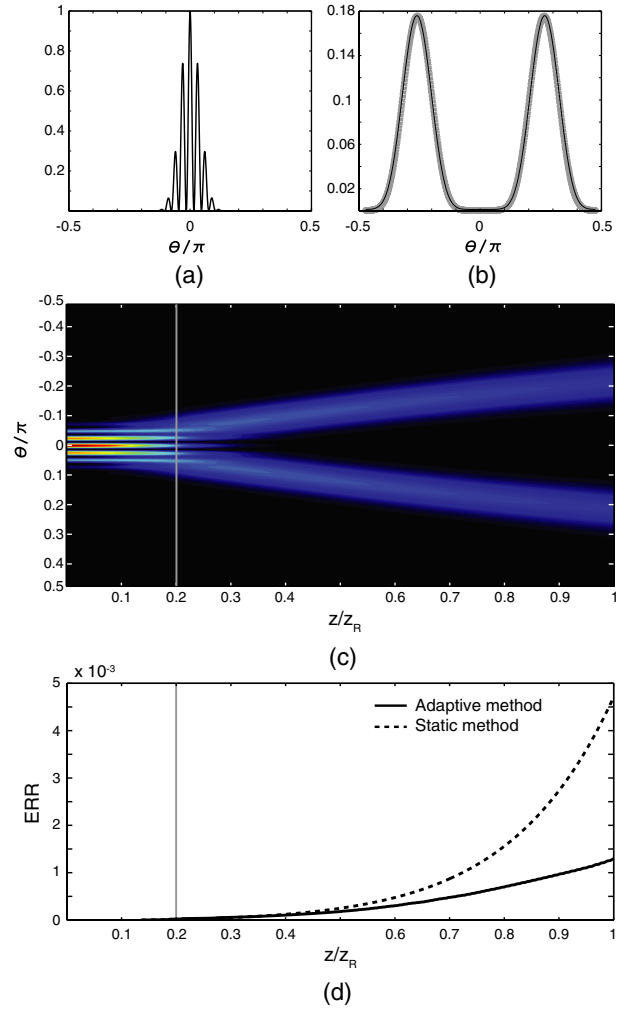

Fig. 3. (Color online) (a) Cosine-Gauss field at $z = 0$. (b) Comparison between the analytical solution (solid black curve) and the numerical solution using our adaptive method (gray dots) at $z = z_R$. (c) Propagation of the cosine-Gauss field in the plane (θ, z). (d) ERR function [Eq. (16)] for the proposed adaptive boundary method and the standard static method.

which provides a measure of error in the shape and numerical dissipation.

For the adaptive method, the procedure is as follows: after each propagation, we calculate the position x_0 of the maximum intensity for the field U. Then, we obtain our new sampling points using Eq. (2) with $\theta_0 = \tan^{-1}(x_0/\alpha)$. The values of U at the new sampling points are calculated by spline cubic interpolation. Finally, Eq. (8) is solved to find the next solution of U. Since the implicit Crank–Nicolson scheme that we use for the solution of Eq. (8) requires calculation of an inverse matrix, the adaptive method takes additional computational work at each propagation step. However, we can monitor x_0 after each propagation and evaluate its variation with respect to the previous solution, in order to decide if we should change the grid. An important characteristic of the mapping transformation using the tangent function is that the matrix elements of Eq. (8) present small variations at each step. This produces a well-scaled matrix and its inverse can be efficiently calculated. Other mapping functions could produce badly scaled matrices and the method becomes inefficient. Another alternative is to use explicit methods to avoid the inverse matrix calculation. This could reduce the computation time but the method becomes conditionally stable, and the stability should be monitored each propagation step.

Figure 3(c) shows the overlap error [Eq. (16)] as a function of the propagation distance z for both methods. The field behaves as a pseudo-nondiffracting beam during a distance of about 1 m ($z/z_R \approx 0.2$) before evolving into two tilted Gaussian beams. The separation angle is defined by k_t. In the nondiffracting region both methods are equivalents since the high field amplitude is along the propagation direction and therefore $r_m = 0$ and $\theta_m = 0$.

After that region, both methods start to differ. Here, our adaptive method concentrates the higher density of sampling points along the direction of each Gaussian beam. In the static case, however, the number of points sampling the Gaussian beams reduces, thus increasing the numerical error. The adaptive method presents better results for long propagation, compared to the static boundaryless method. This method is useful for propagation along complex optical systems, where the energy concentration changes after each optical element.

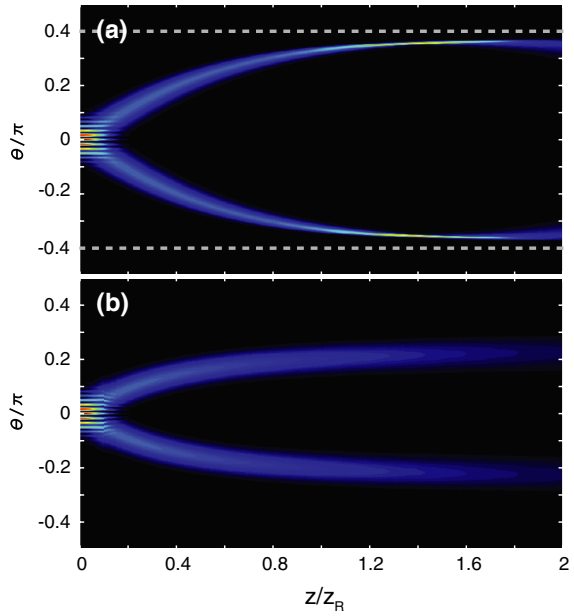

Fig. 4. (Color online) (a) Long propagation of the cosine-Gauss beam using the standard static method. The dotted lines show the fictitious boundary produced by frequency aliasing due to the scarcely sampled region. (b) Long propagation using our adaptive method, showing better performance than the standard method.

The static method suffers from frequency aliasing when the sampling interval is larger than $\Delta x = \pi/k_t$. Figure 4(a) shows an example of this problem. In this case we use a $k_t/k = 15 \times 10^{-4}$, which produces a fictitious boundary about $|\theta|/\pi \approx 0.4$. Small reflections from this fictitious boundary accumulate at about $z/z_R \approx 1.4$, which produces a local intensity peak.

Figure 4(b) shows the propagation obtained with our adaptive method. The solution does not present reflections from an artificial boundary as in the static case. This allows us to propagate our solution along larger distances. For this case we use $\theta_{\max} = \pi/2 + \theta_0$ in order to keep $x_{\max}$ at infinite. Notice that, due to the recalculation of the grid, the transverse resolution changes at each propagation step.

4. CONCLUSIONS

We have presented an adaptive boundaryless method that extend the scheme proposed by Ladouceur. This method is useful for problems where the maximum energy concentration differs from the central region. It does not require a previous knowledge of the geometry of the system. The grid adapts according to the distribution of energy at each propagation step.

We have compared the adaptive method with the standard static method. The former shows better results for problems involving tilted waves. Additionally, the adaptive method is not limited by the frequency aliasing problem and shows a good performance for long propagation distances.

The limitation of our method is the requirement of interpolation after each propagation step. This increases the computational time. The method can be extended for wide angle propagation schemes [12], three-dimensional wave propagation [6], or using different approaches to solve the modified wave equation [14].

APPENDIX A: ADAPTIVE METHOD IN CYLINDRICAL COORDINATES

The adaptive boundaryless method can be extended for propagation in (2 + 1)D. For reference, we present the modified paraxial wave equation in cylindrical coordinates using the adaptive mapping function. The paraxial equation in cylindrical coordinates (r, φ, z) is given by

$$\frac{1}{r}\frac{\partial}{\partial r}\left[r\frac{\partial \psi}{\partial r}\right] + 2ik\frac{\partial \psi}{\partial z} - \frac{l^2}{r^2}\psi = 0, \tag{A1}$$

where we assume azimuthal symmetry in the field, namely,

$$U(r, \phi, z) = \psi(r, z)\exp(il\phi). \tag{A2}$$

Using the mapping function $r(\theta) = r_0 + \alpha\tan(\theta - \theta_0)$, we obtain the modified paraxial equation

$$A(\theta)\frac{\partial^2 \psi}{\partial \theta^2} + B(\theta)\frac{\partial \psi}{\partial \theta} + C(\theta)\psi + 2ik\frac{\partial \psi}{\partial z} = 0 \tag{A3}$$

with

$$A(\theta) = \frac{1}{\alpha^2}\cos(\theta-\theta_0)^4, \tag{A4}$$

$$B(\theta) = -\frac{2}{\alpha^2}\cos(\theta-\theta_0)^3\sin(\theta-\theta_0) + \frac{\cos(\theta-\theta_0)^2}{\alpha r(\theta)}, \tag{A5}$$

$$C(\theta) = -\frac{l^2}{r(\theta)^2}. \tag{A6}$$

We can use a field transformation as in the Cartesian coordinates, but the resulting transformation requires an infinite boundary condition at $r = 0$. Therefore, it is convenient to omit the field transformation.

We solve Eq. (A3) using the Crank–Nicolson scheme. The finite-difference equations are

$$\begin{aligned} a_p\psi_{p-1}^{(n+1)} + \left[b_p + \frac{4ik}{\Delta z}\right]\psi_p^{(n+1)} + c_p\psi_{p+1}^{(n+1)} \\ = -a_p\psi_{p-1}^{(n)} - \left[b_p - \frac{4ik}{\Delta z}\right]\psi_p^{(n)} - c_p\psi_{p+1}^{(n)}, \end{aligned} \tag{A7}$$

where

$$a_p = \frac{A(\theta_p)}{\Delta\theta^2} - \frac{B(\theta_p)}{2\Delta\theta}, \tag{A8}$$

$$b_p = -\frac{2A(\theta_p)}{\Delta\theta^2} + C(\theta_p), \tag{A9}$$

$$c_p = \frac{A(\theta_p)}{\Delta\theta^2} + \frac{B(\theta_p)}{2\Delta\theta}. \tag{A10}$$

Equation (A7) can be solved by expressing them in matrix form, similar to Eq. (11).

ACKNOWLEDGMENTS

We acknowledge support from the Consejo Nacional de Ciencia y Tecnología (Grant No. 182005) and from the Tecnológico de Monterrey (Grant No. CAT141).

REFERENCES

1. C. Vassallo and F. Collino, "Highly efficient absorbing boundary conditions for the beam propagation method," J. Lightwave Technol. **14**, 1570–1577 (1996).
2. G. R. Hadley, "Transparent boundary condition for beam propagation," Opt. Lett. **16**, 624–626 (1991).
3. J. P. Berenger, "A perfectly matched layer for the absorption of electromagnetic waves," J. Comput. Phys. **114**, 185–200 (1994).
4. F. Ladouceur, "Boundaryless beam propagation," Opt. Lett. **21**, 4–5 (1996).
5. J. Shibayama, K. Matsubara, M. Sekiguchi, J. Yamauchi, and H. Nakano, "Efficient nonuniform schemes for paraxial and wide-angle finite-difference beam propagation methods," J. Lightwave Technol. **17**, 677–683 (1999).
6. M. Guizar-Sicairos and J. C. Gutiérrez-Vega, "Boundaryless finite-difference method for three-dimensional beam propagation," J. Opt. Soc. Am. A **23**, 866–871 (2006).
7. J. P. Hugonin, P. Lalanne, I. del Villar, and I. R. Matias, "Fourier modal methods for modeling optical dielectric waveguides," Opt. Quantum Electron. **37**, 107–119 (2005).
8. G. C. des Francs, J. P. Hugonin, and J. Čtyroký, "Mode solvers for very thin long-range plasmonic waveguides," Opt. Quantum Electron. **42**, 557–570 (2011).
9. C. Pozrikidis, *Numerical Computation in Science and Engineering* (Oxford, 1998).
10. A. Taflove and S. C. Hagness, *Computational Electrodynamics* (Artech House, 2005).
11. J. C. Gutiérrez-Vega and M. A. Bandres, "Helmholtz–Gauss waves," J. Opt. Soc. Am. A **22**, 289–298 (2005).
12. G. R. Hadley, "Wide-angle beam propagation using Padé approximant operators," Opt. Lett. **17**, 1426–1428 (1992).
13. I. Ilić, R. Scarmozzino, and R. M. Osgood, Jr., "Investigation of the Padé approximant-based wide-angle beam propagation method for accurate modeling of waveguiding circuits," J. Lightwave Technol. **14**, 2813–2822 (1996).
14. A. Sharma and A. Agrawal, "A new finite-difference-based method for wide-angle beam propagation," IEEE Photon. Technol. Lett. **18**, 944–946 (2006).